

Published in final edited form as:

*Nature.* ; 486(7403): 346–352. doi:10.1038/nature10983.

## The genomic and transcriptomic architecture of 2,000 breast tumours reveals novel subgroups

Christina Curtis<sup>1,2,†,\*</sup>, Sohrab P. Shah<sup>3,4,\*</sup>, Suet-Feung Chin<sup>1,2,\*</sup>, Gulisa Turashvili<sup>3,4,\*</sup>, Oscar M. Rueda<sup>1,2</sup>, Mark J. Dunning<sup>2</sup>, Doug Speed<sup>2,5,†</sup>, Andy G. Lynch<sup>1,2</sup>, Shamith Samarajiwa<sup>1,2</sup>, Yinyin Yuan<sup>1,2</sup>, Stefan Gräf<sup>1,2</sup>, Gavin Ha<sup>3</sup>, Gholamreza Haffari<sup>3</sup>, Ali Bashashati<sup>3</sup>, Roslin Russell<sup>2</sup>, Steven McKinney<sup>3,4</sup>, METABRIC Group<sup>†</sup>, Anita Langerød<sup>6</sup>, Andrew Green<sup>7</sup>, Elena Provenzano<sup>8</sup>, Gordon Wishart<sup>8</sup>, Sarah Pinder<sup>9</sup>, Peter Watson<sup>3,4,10</sup>, Florian Markowetz<sup>1,2</sup>, Leigh Murphy<sup>10</sup>, Ian Ellis<sup>7</sup>, Arnie Purushotham<sup>9,11</sup>, Anne-Lise Børresen-Dale<sup>6,12</sup>, James D. Brenton<sup>2,13</sup>, Simon Tavaré<sup>1,2,5,14</sup>, Carlos Caldas<sup>1,2,8,13</sup>, and Samuel Aparicio<sup>3,4</sup>

<sup>1</sup>Department of Oncology, University of Cambridge, Hills Road, Cambridge CB2 2XZ, UK.

<sup>2</sup>Cancer Research UK, Cambridge Research Institute, Li Ka Shing Centre, Robinson Way, Cambridge CB2 0RE, UK.

<sup>3</sup>Department of Pathology and Laboratory Medicine, University of British Columbia, Vancouver, British Columbia V6T 2B5, Canada.

<sup>4</sup>Molecular Oncology, British Columbia Cancer Research Centre, Vancouver, British Columbia V5Z 1L3, Canada.

<sup>5</sup>Department of Applied Mathematics and Theoretical Physics, University of Cambridge, Centre for Mathematical Sciences, Cambridge CB3 0WA, UK.

<sup>6</sup>Department of Genetics, Institute for Cancer Research, Oslo University Hospital Radiumhospitalet, Montebello, 0310 Oslo, Norway.

<sup>7</sup>Department of Histopathology, School of Molecular Medical Sciences, University of Nottingham, Nottingham NG5 1PB, UK.

©2012 Macmillan Publishers Limited. All rights reserved

Correspondence and requests for materials should be addressed to Ca.C. (carlos.caldas@cancer.org.uk) or S.A. (saparicio@bccrc.ca).

<sup>†</sup>Present addresses: Department of Preventive Medicine, Keck School of Medicine, University of Southern California, Los Angeles, California 90033, USA (Ch.C.); University College London, Genetics Institute, WC1E 6BT, UK (D.S.).

\*These authors contributed equally to this work.

<sup>‡</sup>Lists of participants and affiliations appear at the end of the paper.

Supplementary Information is linked to the online version of the paper at [www.nature.com/nature](http://www.nature.com/nature).

**Author Contributions** Ch.C. led the analysis, designed experiments and wrote the manuscript. S.P.S. led the HMM-based analyses, expression outlier and *TP53* analyses, and contributed to manuscript preparation. S.-F.C. generated data, designed and performed experiments. G.T. generated data, provided histopathology expertise and analysed *TP53* sequence data. O.M.R., M.J.D., D.S., A.G.L., S.S., Y.Y., S.G., Ga.H., Gh.H., A.B., R.R., S.M. and F.M. performed analyses. G.T., A.G., E.P., S.P. and I.E. provided histopathology expertise. A.L. performed *TP53* sequencing. A.-L.B.-D. oversaw *TP53* sequencing. S.P., P.W., L.M., G.W., I.E., A.P., Ca.C. and S.A. contributed to sample selection. J.D.B. and S.T. contributed to study design. S.T. provided statistical expertise. The METABRIC Group contributed collectively to this study. Ca.C. and S.A. co-conceived and oversaw the study, and contributed to manuscript preparation and were responsible for final editing. Ca.C. and S.A. are joint senior authors and project co-leaders.

The authors declare no competing financial interests.

**Author Information** The associated genotype and expression data have been deposited at the European Genome-Phenome Archive (<http://www.ebi.ac.uk/ega/>), which is hosted by the European Bioinformatics Institute, under accession number EGAS00000000083. Reprints and permissions information is available at [www.nature.com/reprints](http://www.nature.com/reprints). Readers are welcome to comment on the online version of this article at [www.nature.com/nature](http://www.nature.com/nature).

<sup>8</sup>Cambridge Breast Unit, Addenbrooke's Hospital, Cambridge University Hospital NHS Foundation Trust and NIHR Cambridge Biomedical Research Centre, Cambridge CB2 2QQ, UK.

<sup>9</sup>King's College London, Breakthrough Breast Cancer Research Unit, London WC2R 2LS, UK.

<sup>10</sup>Manitoba Institute of Cell Biology, University of Manitoba, Manitoba R3E 0V9, Canada.

<sup>11</sup>NIHR Comprehensive Biomedical Research Centre at Guy's and St Thomas' NHS Foundation Trust and King's College London, London WC2R 2LS, UK.

<sup>12</sup>Institute for Clinical Medicine, Faculty of Medicine, University of Oslo, 0316 Oslo, Norway.

<sup>13</sup>Cambridge Experimental Cancer Medicine Centre, Cambridge CB2 0RE, UK.

<sup>14</sup>Molecular and Computational Biology Program, University of Southern California, Los Angeles, California 90089, USA.

## Abstract

The elucidation of breast cancer subgroups and their molecular drivers requires integrated views of the genome and transcriptome from representative numbers of patients. We present an integrated analysis of copy number and gene expression in a discovery and validation set of 997 and 995 primary breast tumours, respectively, with long-term clinical follow-up. Inherited variants (copy number variants and single nucleotide polymorphisms) and acquired somatic copy number aberrations (CNAs) were associated with expression in ~40% of genes, with the landscape dominated by *cis*- and *trans*-acting CNAs. By delineating expression outlier genes driven in *cis* by CNAs, we identified putative cancer genes, including deletions in *PPP2R2A*, *MTAP* and *MAP2K4*. Unsupervised analysis of paired DNA–RNA profiles revealed novel subgroups with distinct clinical outcomes, which reproduced in the validation cohort. These include a high-risk, oestrogen-receptor-positive 11q13/14 *cis*-acting subgroup and a favourable prognosis subgroup devoid of CNAs. *Trans*-acting aberration hotspots were found to modulate subgroup-specific gene networks, including a TCR deletion-mediated adaptive immune response in the 'CNA-devoid' subgroup and a basal-specific chromosome 5 deletion-associated mitotic network. Our results provide a novel molecular stratification of the breast cancer population, derived from the impact of somatic CNAs on the transcriptome.

---

Inherited genetic variation and acquired genomic aberrations contribute to breast cancer initiation and progression. Although somatically acquired CNAs are the dominant feature of sporadic breast cancers, the driver events that are selected for during tumorigenesis are difficult to elucidate as they co-occur alongside a much larger landscape of random non-pathogenic passenger alterations<sup>1,2</sup> and germline copy number variants (CNVs). Attempts to define subtypes of breast cancer and to discern possible somatic drivers are still in their relative infancy<sup>3–6</sup>, in part because breast cancer represents multiple diseases, implying that large numbers (many hundreds or thousands) of patients must be studied. Here we describe an integrated genomic/transcriptomic analysis of breast cancers with long-term clinical outcomes composed of a discovery set of 997 primary tumours and a validation set of 995 tumours from METABRIC (Molecular Taxonomy of Breast Cancer International Consortium).

## A breast cancer population genomic resource

We assembled a collection of over 2,000 clinically annotated primary fresh-frozen breast cancer specimens from tumour banks in the UK and Canada (Supplementary Tables 1–3). Nearly all oestrogen receptor (ER)-positive and/or lymph node (LN)-negative patients did not receive chemotherapy, whereas ER-negative and LN-positive patients did. Additionally, none of the HER2<sup>+</sup> patients received trastuzumab. As such, the treatments were

homogeneous with respect to clinically relevant groupings. An initial set of 997 tumours was analysed as a discovery group and a further set of 995 tumours, for which complete data later became available, was used to test the reproducibility of the integrative clusters (described below). An overview of the main analytical approaches is provided in Supplementary Fig. 1. Details concerning expression and copy number profiling, including sample assignment to the PAM50 intrinsic subtypes<sup>3,4,7</sup> (Supplementary Fig. 2), copy number analysis (Supplementary Tables 4–8) and validation (Supplementary Figs 3 and 4 and Supplementary Tables 9–11), and *TP53* mutational profiling (Supplementary Fig. 5) are described in the Supplementary Information.

## Genome variation affects tumour expression architecture

Genomic variants are considered to act in *cis* when a variant at a locus has an impact on its own expression, or in *trans* when it is associated with genes at other sites in the genome. We generated a map of CNAs, CNVs (Supplementary Fig. 6, Supplementary Tables 12–15) and single nucleotide polymorphisms (SNPs) in the breast cancer genome to distinguish germline from somatic variants (see Methods), and to examine the impact of each of these variants on the expression landscape. Previous studies<sup>8</sup> have shown that most heritable gene expression traits are governed by a combination of *cis* (proximal) loci, defined here as those within a 3-megabase (Mb) window surrounding the gene of interest, and *trans* (distal) loci, defined here as those outside that window. We assessed the relative influence of SNPs, CNVs and CNAs on tumour expression architecture, using each of these variants as a predictor (see Methods) to elucidate expression quantitative trait loci (eQTLs) among patients.

Both germline variants and somatic aberrations were found to influence tumour expression architecture, having an impact on >39% (11,198/28,609) of expression probes genome-wide based on analysis of variance (ANOVA; see Methods), with roughly equal numbers of genes associated in *cis* and *trans*. CNAs were associated with the greatest number of expression profiles (Fig. 1, Supplementary Figs 7–13 and Supplementary Tables 16–20), but were rivalled by SNPs to explain a greater proportion of expression variation on a per-gene basis genome-wide, whereas the contribution from CNVs was more moderate (Fig. 1b and Supplementary Table 21). The true ratio of putative *trans* versus *cis* eQTLs is hard to estimate<sup>9</sup>; however, the large sample size used here allowed the detection of small effects, with 5,401 and 5,462 CNAs significantly (Šidák adjusted *P* value <0.0001) associated in *cis* or in *trans*, respectively. Whereas *cis*-associations tended to be stronger, the *trans*-acting loci modulated a larger number of messenger RNAs, as described below.

## Expression outliers refine the breast cancer landscape

As shown above, ~20% of loci exhibit CNA-expression associations in *cis* (Supplementary Fig. 14). To refine this landscape further and identify the putative driver genes, we used profiles of outlying expression (see Methods and ref. 10) and the high resolution and sensitivity of the Affymetrix SNP 6.0 platform to delineate candidate regions. This approach markedly reduces the complexity of the landscape to 45 regions (frequency > 5, Fig. 2) and narrows the focus, highlighting novel regions that modulate expression. The full enumeration of regions delineated by this approach and their subtype-specific associations (Supplementary Figs 15 and 16 and Supplementary Tables 22–24) includes both known drivers (for example, *ZNF703* (ref. 11), *PTEN* (ref. 12), *MYC*, *CCND1*, *MDM2*, *ERBB2*, *CCNE1* (ref. 13)) and putative driver aberrations (for example, *MDM1*, *MDM4*, *CDK3*, *CDK4*, *CAMK1D*, *PI4KB*, *NCOR1*).

The deletion landscape of breast cancer has been poorly explored, with the exception of *PTEN*. We illustrate three additional regions of significance centred on *PPP2R2A* (8p21,

Fig. 2, region 11), *MTAP* (9p21, Fig. 2, region 15) and *MAP2K4* (17p11, Fig. 2, region 33), which exhibit heterozygous and homozygous deletions (Supplementary Figs 15, 17–19 and Supplementary Table 24) that drive expression of these loci. We observe breast cancer subtype-specific (enriched in mitotic ER-positive cancers) loss of transcript expression in *PPP2R2A*, a B-regulatory subunit of the PP2A mitotic exit holoenzyme complex. Somatic mutations in *PPP2R1A* have recently been reported in clear cell ovarian cancers and endometrioid cancers<sup>14,15</sup>, and methylation silencing of *PPP2R2B* has also been observed in colorectal cancers<sup>16</sup>. Thus, dysregulation of specific PPP2R2A functions in luminal B breast cancers adds a significant pathophysiology to this subtype.

*MTAP* (9p21, a component of methyladenosine salvage) is frequently co-deleted with the *CDKN2A* and *CDKN2B* tumour suppressor genes in a variety of cancers<sup>17</sup> as we observe here (Supplementary Figs 17c and 18). The third deletion encompasses *MAP2K4* (also called *MKK4*) (17p11), a p38/Jun dual specificity serine/threonine protein kinase. *MAP2K4* has been proposed as a recessive cancer gene<sup>18</sup>, with mutations noted in cell lines<sup>19</sup>. We show, for the first time, the recurrent deletion of *MAP2K4* (Supplementary Figs 17d and 19) concomitant with outlying expression (Supplementary Fig. 15) in predominantly ER-positive cases, and verify homozygous deletions (Supplementary Table 9) in primary tumours, strengthening the evidence for *MAP2K4* as a tumour suppressor in breast cancer.

### Trans-acting associations reveal distinct modules

We next asked how *trans*-associated expression profiles are distributed across the genome. We mapped these in the expression landscape by examining the matrices of CNA–expression associations (see Methods). This revealed strong off-diagonal patterns at loci on chromosomes 1q, 7p, 8, 11q, 14q, 16, 17q and 20q (Fig. 3a), including both positive and negative associations, as well as numerous *trans*-acting aberration hotspots (defined as CNAs associated with >30 mRNAs). Importantly, these aberration hotspots can be grouped into pathway modules, which highlight known driver loci such as *ERBB2* and *MYC*, as well as novel loci associated with large *trans* expression modules (Supplementary Tables 25 and 26). The T-cell-receptor (TCR) loci on chromosomes 7 (*TRG*) and 14 (*TRA*) represent two such hotspots that modulated 381 and 153 unique mRNAs, respectively, as well as 19 dually regulated genes (Supplementary Fig. 20). These cognate mRNAs were highly enriched for T-cell activation and proliferation, dendritic cell presentation, and leukocyte activation, which indicate the induction of an adaptive immune response associated with tumour-infiltrating lymphocytes (Fig. 3b, Supplementary Fig. 20 and Supplementary Tables 27 and 28), as described later.

In a second approach, we examined the genome-wide patterns of linear correlation between copy number and expression features (see Methods), and noted the alignment of several off-diagonal signals, including those on chromosome 1q, 8q, 11q, 14q and 16 (Supplementary Fig. 21). Additionally, a broad signal on chromosome 5 localizing to a deletion event restricted to the basal-like tumours was observed (Supplementary Fig. 21), but was not detected with the eQTL framework, where discrete (as opposed to continuous) copy number values were used. This basal-specific *trans* module is enriched for transcriptional changes involving cell cycle, DNA damage repair and apoptosis (Supplementary Table 29), reflecting the high mitotic index typically associated with basal-like tumours, described in detail below.

### Integrative clustering reveals novel subgroups

Using the discovery set of 997 breast cancers, we next asked whether novel biological subgroups could be found by joint clustering of copy number and gene expression data. On the basis of our finding that *cis*-acting CNAs dominated the expression landscape, the top

1,000 *cis*-associated genes across all subtypes (Supplementary Table 30) were used as features for input to a joint latent variable framework for integrative clustering<sup>20</sup> (see Methods). Cluster analysis suggested 10 groups (based on Dunn's index) (see Methods and Supplementary Figs 22 and 23), but for completeness, this result was compared with the results for alternative numbers of clusters and clustering schemes (see Methods, Supplementary Figs 23–27 and Supplementary Tables 31–33). The 10 integrative clusters (labelled IntClust 1–10) were typified by well-defined copy number aberrations (Fig. 4, Supplementary Figs 22, 28–30 and Supplementary Tables 34–39), and split many of the intrinsic subtypes (Supplementary Figs 31–33). Kaplan–Meier plots of disease-specific survival and Cox proportional hazards models indicate subgroups with distinct clinical outcomes (Fig. 5, Supplementary Figs 34, 35 and Supplementary Tables 40 and 41). To validate these results, we trained a classifier (754 features) for the integrative subtypes in the discovery set using the nearest shrunken centroids approach<sup>21</sup> (see Methods and Supplementary Tables 42 and 43), and then classified the independent validation set of 995 cases into the 10 groups (Supplementary Table 44). The reproducibility of the clusters in the validation set is shown in three ways. First, classification of the validation set resulted in the assignment of a similar proportion of cases to the 10 subgroups, each of which exhibited nearly identical copy number profiles (Fig. 4). Second, the groups have substantially similar hazard ratios (Fig. 5b, Supplementary Fig. 35 and Supplementary Table 40). Third, the quality of the clusters in the validation set is emphasized by the in-group proportions (IGP) measure<sup>22</sup> (Fig. 4).

Among the integrative clusters, we first note an ER-positive subgroup composed of 11q13/14 *cis*-acting luminal tumours (IntClust 2,  $n = 45$ ) that harbour other common alterations. This subgroup exhibited a steep mortality trajectory with elevated hazard ratios (discovery set: 3.620, 95% confidence interval (1.905–6.878); validation set: 3.353, 95% confidence interval (1.381–8.141)), indicating that it represents a particularly high-risk subgroup. Several known and putative driver genes reside in this region, namely *CCND1* (11q13.3), *EMSY* (11q13.5), *PAK1* (11q14.1) and *RSF1* (11q14.1), which have been previously linked to breast<sup>13,23</sup> or ovarian cancer<sup>24</sup>. Both the copy number (Fig. 4) and expression outlier landscapes (Fig. 2) suggest at least two separate amplicons at 11q13/14, one at *CCND1* (11q13.3) and a separate peak from 11q13.5–11q14.1 spanning *UVRAG–GAB2*, centred around *PAK1*, *RSF1*, *C11orf67* and *INTS4*, where it is more challenging to distinguish the driver<sup>24</sup>. Notably, the expression outlier profiles for this region are enriched for samples belonging to IntClust 2 (Fig. 2, inset region 23) and all 45 members of this subgroup harboured amplifications of these genes, with high frequencies of amplification also observed for *CCND1* ( $n = 39$ ) and *EMSY* ( $n = 34$ ). In light of these observations, the 11q13/14 amplicon may be driven by a cassette of genes rather than a single oncogene.

Second, we note the existence of two subgroups marked by a paucity of copy number and *cis*-acting alterations. These subgroups cannot be explained by low cellularity tumours (see Methods). One subgroup (IntClust3,  $n = 156$ ) with low genomic instability (Fig. 4 and Supplementary Fig. 22) was composed predominantly of luminal A cases, and was enriched for histotypes that typically have good prognosis, including invasive lobular and tubular carcinomas. The other subgroup (IntClust 4,  $n = 167$ ) was also composed of favourable outcome cases, but included both ER-positive and ER-negative cases and varied intrinsic subtypes, and had an essentially flat copy number landscape, hence termed the 'CNA-devoid' subgroup. A significant proportion of cases within this subgroup exhibit extensive lymphocytic infiltration (Supplementary Table 45).

Third, several intermediate prognosis groups of predominantly ER-positive cancers were identified, including a 17q23/20q *cis*-acting luminal B subgroup (IntClust 1,  $n = 76$ ), an 8p12 *cis*-acting luminal subgroup (IntClust 6,  $n = 44$ ), as well as an 8q *cis*-acting/20q-

amplified mixed subgroup (IntClust 9,  $n = 67$ ). Two luminal A subgroups with similar CNA profiles and favourable outcome were noted. One subgroup is characterized by the classical 1q gain/16q loss (IntClust 8,  $n = 143$ ), which corresponds to a common translocation event<sup>25</sup>, and the other lacks the 1q alteration, while maintaining the 16p gain/16q loss with higher frequencies of 8q amplification (IntClust 7,  $n = 109$ ). We also noted that the majority of basal-like tumours formed a stable, mostly high-genomic instability subgroup (IntClust 10,  $n = 96$ ). This subgroup had relatively good long-term outcomes (after 5 years), consistent with ref. 26, and characteristic *cis*-acting alterations (5 loss/8q gain/10p gain/12p gain).

The *ERBB2*-amplified cancers composed of HER2-enriched (ER-negative) cases and luminal (ER-positive) cases appear as IntClust 5 ( $n = 94$ ), thus refining the *ERBB2* intrinsic subtype by grouping additional patients that might benefit from targeted therapy. Patients in this study were enrolled before the general availability of trastuzumab, and as expected this subgroup exhibits the worst disease-specific survival at both 5 and 15 years and elevated hazard ratios (discovery set: 3.899, 95% confidence interval (2.234–6.804); validation set: 4.447, 95% confidence interval (2.284–8.661)).

## Pathway deregulation in the integrative subgroups

Finally, we projected the molecular profiles of the integrative subgroups onto pathways to examine possible biological themes among breast cancer subgroups (Supplementary Tables 46 and 47) and the relative impact of *cis* and *trans* expression modules on the pathways. The CNA-devoid (IntClust 4) group exhibits a strong immune and inflammation signature involving the antigen presentation pathway, OX40 signalling, and cytotoxic T-lymphocyte-mediated apoptosis (Supplementary Fig. 36). Given that *trans*-acting deletion hotspots were localized to the *TRG* and *TRA* loci and were associated with an adaptive immune response module, we asked whether these deletions contribute to alterations in this pathway. The CNA-devoid subgroup (IntClust 4) was found to exhibit nearly twice as many deletions (typically heterozygous loss) at the *TRG* and *TRA* loci (~20% of cases) as compared to the other subtypes (with the exception of IntClust 10), and deletions of both TCR loci were significantly associated with severe lymphocytic infiltration ( $\chi^2$  test,  $P < 10^{-9}$  and  $P < 10^{-8}$ , respectively). Notably, these *trans*-associated mRNAs were significantly enriched in the immune response signature of the CNA-devoid subgroup (Supplementary Fig. 36) as well as among genes differentially expressed in CNA-devoid cases with severe lymphocytic infiltration (Supplementary Fig. 37). We conclude that genomic copy number loss at the TCR loci drives a *trans*-acting immune response module that associates with lymphocytic infiltration, and characterizes an otherwise genomically quiescent subgroup of ER-positive and ER-negative patients with good prognosis. These observations suggest the presence of mature T lymphocytes (with rearranged TCR loci), which may explain an immunological response to the cancer. In line with these findings, a recent study<sup>27</sup> demonstrated the association between CD8<sup>+</sup> lymphocytes and favourable prognosis.

Also among the *trans*-influenced groups is IntClust 10 (basal-like cancer enriched subgroup), which harbours chromosome 5q deletions (Supplementary Fig. 21). Numerous signalling molecules, transcription factors and cell division genes were associated in *trans* with this deletion event in the basal cancers, including alterations in *AURKB*, *BCL2*, *BUB1*, *CDCA3*, *CDCA4*, *CDC20*, *CDC45*, *CHEK1*, *FOXM1*, *HDAC2*, *IGF1R*, *KIF2C*, *KIFC1*, *MTHFD1L*, *RAD51API*, *TTK* and *UBE2C* (Supplementary Fig. 38). Notably, *TTK* (*MPS1*), a dual specificity kinase that assists *AURKB* in chromosome alignment during mitosis, and recently reported to promote aneuploidy in breast cancer<sup>28</sup>, was upregulated. These results indicate that 5q deletions modulate the coordinate transcriptional control of genomic and chromosomal instability and cell cycle regulation within this subgroup.

In contrast to these subtype-specific *trans*-associated signatures, the high-risk 11q13/14 subgroup was characterized by strong *cis*-acting associations. Like the basal cancers, this subgroup also exhibited alterations in key cell-cycle-related genes (Supplementary Fig. 39), which probably have a role in its aggressive pathophysiology, but the nature of the signature differs. In particular, the regulation of the G1/S transition by BTG family proteins, which include *CCND1*, *PPP2R1B* and *E2F2*, was significantly enriched in the 11q13/14 *cis*-acting subgroup, but not the basal cancers, and this is consistent with *CCND1* and the *PPP2R* subunit representing subtype-specific drivers in these tumours.

## Discussion

We have generated a robust, population-based molecular subgrouping of breast cancer based on multiple genomic views. The size and nature of this cohort made it amenable to eQTL analyses, which can aid the identification of loci that contribute to the disease phenotype<sup>29</sup>. CNAs and SNPs influenced expression variation, with CNAs dominating the landscape in *cis* and *trans*. The joint clustering of CNAs and gene expression profiles further resolves the considerable heterogeneity of the expression-only subgroups, and highlights a high-risk 11q13/14 *cis*-acting subgroup as well as several other strong *cis*-acting clusters and a genomically quiescent group. The reproducibility of subgroups with these molecular and clinical features in a validation cohort of 995 tumours suggests that by integrating multiple genomic features it may be possible to derive more robust patient classifiers. We show here, for the first time, that subtype-specific *trans*-acting aberrations modulate concerted transcriptional changes, such as the TCR deletion-mediated adaptive immune response that characterizes the CNA-devoid subgroup and the chromosome 5 deletion-associated cell cycle program in the basal cancers.

The integrated CNA-expression landscape highlights a limited number of genomic regions that probably contain driver genes, including *ZNF703*, which we recently described as a luminal B specific driver<sup>11</sup>, as well as somatic deletion events affecting key subunits of the PP2A holoenzyme complex and *MTAP*, which have previously been under-explored in breast cancer. The CNA-expression landscape also illuminates rare but potentially significant events, including *IGF1R*, *KRAS* and *EGFR* amplifications and *CDKN2B*, *BRCA2*, *RB1*, *ATM*, *SMAD4*, *NCOR1* and *UTX* homozygous deletions. Although some of these events have low overall frequencies (<1% patients) (Figs 2, Supplementary Fig. 15 and Supplementary Tables 22–24), they may have implications for understanding therapeutic responses to targeted agents, particularly those targeting tyrosine kinases or phosphatases.

Finally, because the integrative subgroups occur at different frequencies in the overall population, focusing sequencing efforts on representative numbers from these groups will help to establish a comprehensive breast cancer somatic landscape at sequence-level resolution. For example, a significant number (~17%,  $n = 167$  in the discovery cohort) of breast cancers are devoid of somatic CNAs, and are ripe for mutational profiling. Our work provides a definitive framework for understanding how gene copy number aberrations affect gene expression in breast cancer and reveals novel subgroups that should be the target of future investigation.

## METHODS SUMMARY

All patient specimens were obtained with appropriate consent from the relevant institutional review board. DNA and RNA were isolated from samples and hybridized to the Affymetrix SNP 6.0 and Illumina HT-12 v3 platforms for genomic and transcriptional profiling, respectively. A detailed description of the experimental assays and analytical methods used to analyse these data are available in the Supplementary Information.

## Supplementary Material

Refer to Web version on PubMed Central for supplementary material.

## Acknowledgments

The METABRIC project was funded by Cancer Research UK, the British Columbia Cancer Foundation and Canadian Breast Cancer Foundation BC/Yukon. The authors also acknowledge the support of the University of Cambridge, Hutchinson Whampoa, the NIHR Cambridge Biomedical Research Centre, the Cambridge Experimental Cancer Medicine Centre, the Centre for Translational Genomics (CTAG) Vancouver and the BCCA Breast Cancer Outcomes Unit. S.P.S. is a Michael Smith Foundation for Health Research fellow. S.A. is supported by a Canada Research Chair. This work was supported by the National Institutes of Health Centers of Excellence in Genomics Science grant P50 HG02790 (S.T.). The authors thank C. Perou and J.Parker for discussions on the use of the PAM50 centroids. They also acknowledge the patients who donated tissue and the associated pseudo-anonymized clinical data for this project.

## METABRIC Group

**Co-chairs** Carlos Caldas<sup>1,2</sup>, Samuel Aparicio<sup>3,4</sup>

**Writing committee** Christina Curtis<sup>1,2†</sup>, Sohrab P. Shah<sup>3,4</sup>, Carlos Caldas<sup>1,2</sup>, Samuel Aparicio<sup>3,4</sup>

**Steering committee** James D. Brenton<sup>1,2</sup>, Ian Ellis<sup>5</sup>, David Huntsman<sup>3,4</sup>, Sarah Pinder<sup>6</sup>, Arnie Purushotham<sup>6</sup>, Leigh Murphy<sup>7</sup>, Carlos Caldas<sup>1,2</sup>, Samuel Aparicio<sup>3,4</sup>

**Tissue and clinical data source sites: University of Cambridge/Cancer Research UK Cambridge Research Institute** Carlos Caldas (Principal Investigator)<sup>1,2</sup>; Helen Bardwell<sup>2</sup>, Suet-Feung Chin<sup>1,2</sup>, Christina Curtis<sup>1,2†</sup>, Zhihao Ding<sup>2</sup>, Stefan Gräf<sup>1,2</sup>, Linda Jones<sup>8</sup>, Bin Liu<sup>1,2</sup>, Andy G. Lynch<sup>1,2</sup>, Irene Papatheodorou<sup>1,2</sup>, Stephen J. Sammut<sup>9</sup>, Gordon Wishart<sup>9</sup>; **British Columbia Cancer Agency** Samuel Aparicio (Principal Investigator)<sup>3,4</sup>, Steven Chia<sup>4</sup>, Karen Gelmon<sup>4</sup>, David Huntsman<sup>3,4</sup>, Steven McKinney<sup>3,4</sup>, Caroline Speers<sup>4</sup>, Gulisa Turashvili<sup>3,4</sup>, Peter Watson<sup>3,4,7</sup>; **University of Nottingham:** Ian Ellis (Principal Investigator)<sup>5</sup>, Roger Blamey<sup>5</sup>, Andrew Green<sup>5</sup>, Douglas Macmillan<sup>5</sup>, Emad Rakha<sup>5</sup>; **King's College London** Arnie Purushotham (Principal Investigator)<sup>6</sup>, Cheryl Gillett<sup>6</sup>, Anita Grigoriadis<sup>6</sup>, Sarah Pinder<sup>6</sup>, Emanuele de Rinaldis<sup>6</sup>, Andy Tutt<sup>6</sup>; **Manitoba Institute of Cell Biology** Leigh Murphy (Principal Investigator)<sup>7</sup>, Michelle Parisien<sup>7</sup>, Sandra Troup<sup>7</sup>

**Cancer genome/transcriptome characterization centres: University of Cambridge/Cancer Research UK Cambridge Research Institute** Carlos Caldas (Principal Investigator)<sup>1,2</sup>, Suet-Feung Chin (Team Leader)<sup>1,2</sup>, Derek Chan<sup>1</sup>, Claire Fielding<sup>2</sup>, Ana-Teresa Maia<sup>1,2</sup>, Sarah McGuire<sup>2</sup>, Michelle Osborne<sup>2</sup>, Sara M. Sayalero<sup>2</sup>, Inmaculada Spiteri<sup>2</sup>, James Hadfield<sup>2</sup>; **British Columbia Cancer Agency** Samuel Aparicio (Principal Investigator)<sup>3,4</sup>, Gulisa Turashvili (Team Leader)<sup>3,4</sup>, Lynda Bell<sup>4</sup>, Katie Chow<sup>4</sup>, Nadia Gale<sup>4</sup>, David Huntsman<sup>3,4</sup>, Maria Kovalik<sup>4</sup>, Ying Ng<sup>4</sup>, Leah Prentice<sup>4</sup>

**Data analysis subgroup: University of Cambridge/Cancer Research UK Cambridge Research Institute** Carlos Caldas (Principal Investigator)<sup>1,2</sup>, Simon Tavaré (Principal Investigator)<sup>1,2,10,11</sup>, Christina Curtis (Team Leader)<sup>1,2†</sup>, Mark J. Dunning<sup>2</sup>, Stefan Gräf<sup>1,2</sup>, Andy G. Lynch<sup>1,2</sup>, Oscar M. Rueda<sup>1,2</sup>, Roslin Russell<sup>2</sup>, Shamith Samarajiwa<sup>1,2</sup>, Doug Speed<sup>2,10</sup>, Florian Markowitz (Principal Investigator)<sup>1,2</sup>, Yinyin Yuan<sup>1,2</sup>; James D. Brenton (Principal Investigator)<sup>1,2</sup>; **British Columbia Cancer Agency** Samuel Aparicio (Principal Investigator)<sup>3,4</sup>, Sohrab P. Shah (Team Leader)<sup>3,4</sup>, Ali Bashashati<sup>3</sup>, Gavin Ha<sup>3</sup>, Gholamreza Haffari<sup>3</sup> & Steven McKinney<sup>3,4</sup>

<sup>1</sup>Department of Oncology, University of Cambridge, Hills Road, Cambridge CB2 2XZ, UK. <sup>2</sup>Cancer Research UK, Cambridge Research Institute, Li Ka Shing Centre, Robinson Way, Cambridge CB2 0RE, UK. <sup>3</sup>Department of Pathology and Laboratory Medicine, University of British Columbia, Vancouver, British Columbia V6T 2B5, Canada. <sup>4</sup>Molecular Oncology, British Columbia Cancer Research Centre, Vancouver, British Columbia V5Z 1L3, Canada. <sup>5</sup>Department of Histopathology, School of Molecular Medical Sciences, University of Nottingham, Nottingham NG5 1PB, UK. <sup>6</sup>King's College London, Breakthrough Breast Cancer Research Unit, London, WC2R 2LS, UK. <sup>7</sup>Manitoba Institute of Cell Biology, University of Manitoba, Manitoba R3E 0V9, Canada. <sup>8</sup>Cambridge Experimental Cancer Medicine Centre, Cambridge CB2 0RE, UK. <sup>9</sup>Cambridge Breast Unit, Addenbrooke's Hospital, Cambridge University Hospital NHS Foundation Trust and NIHR Cambridge Biomedical Research Centre, Cambridge CB2 2QQ, UK. <sup>10</sup>Department of Applied Mathematics and Theoretical Physics, University of Cambridge, Centre for Mathematical Sciences, Cambridge CB3 0WA, UK. <sup>11</sup>Molecular and Computational Biology Program, University of Southern California, Los Angeles, California 90089, USA. †Present address: Department of Preventive Medicine, Keck School of Medicine, University of Southern California, Los Angeles, California 90033, USA.

## References

1. Leary RJ, et al. Integrated analysis of homozygous deletions, focal amplifications, and sequence alterations in breast and colorectal cancers. *Proc. Natl Acad. Sci. USA.* 2008; 105:16224–16229. [PubMed: 18852474]
2. Bignell GR, et al. Signatures of mutation and selection in the cancer genome. *Nature.* 2010; 463:893–898. [PubMed: 20164919]
3. Perou CM, et al. Molecular portraits of human breast tumours. *Nature.* 2000; 406:747–752. [PubMed: 10963602]
4. Sørlie T, et al. Gene expression patterns of breast carcinomas distinguish tumor subclasses with clinical implications. *Proc. Natl Acad. Sci. USA.* 2001; 98:10869–10874. [PubMed: 11553815]
5. Chin K, et al. Genomic and transcriptional aberrations linked to breast cancer pathophysiologies. *Cancer Cell.* 2006; 10:529–541. [PubMed: 17157792]
6. Chin SF, et al. High-resolution aCGH and expression profiling identifies a novel genomic subtype of ER negative breast cancer. *Genome Biol.* 2007; 8:R215. [PubMed: 17925008]
7. Parker JS, et al. Supervised risk predictor of breast cancer based on intrinsic subtypes. *J. Clin. Oncol.* 2009; 27:1160–1167. [PubMed: 19204204]
8. Stranger BE, et al. Genome-wide associations of gene expression variation in humans. *PLoS Genet.* 2005; 1:e78. [PubMed: 16362079]
9. Gilad Y, Rifkin SA, Pritchard JK. Revealing the architecture of gene regulation: the promise of eQTL studies. *Trends Genet.* 2008; 24:408–415. [PubMed: 18597885]
10. Teschendorff AE, Naderi A, Barbosa-Morais NL, Caldas C. PACK: Profile analysis using clustering and kurtosis to find molecular classifiers in cancer. *Bioinformatics.* 2006; 22:2269–2275. [PubMed: 16682424]
11. Holland D, et al. ZNF703 is a common Luminal B breast cancer oncogene that differentially regulates luminal and basal progenitors in human mammary epithelium. *EMBO Mol. Med.* 2011; 3:167–180. [PubMed: 21337521]
12. Li J, et al. PTEN, a putative protein tyrosine phosphatase gene mutated in human brain, breast, and prostate cancer. *Science.* 1997; 275:1943–1947. [PubMed: 9072974]
13. Santarius T, Shiply J, Brewer D, Stratton MR, Cooper CS. A census of amplified and overexpressed human cancer genes. *Nature Rev. Cancer.* 2010; 10:59–64. [PubMed: 20029424]
14. Jones S, et al. Frequent mutations of chromatin remodeling gene ARID1A in ovarian clear cell carcinoma. *Science.* 2010; 330:228–231. [PubMed: 20826764]
15. McConechy MK, et al. Subtype-specific mutation of PPP2R1A in endometrial and ovarian carcinomas. *J. Pathol.* 2011; 223:567–573. [PubMed: 21381030]

16. Tan J, et al. B55 $\beta$ -associated PP2A complex controls PDK1-directed MYC signaling and modulates rapamycin sensitivity in colorectal cancer. *Cancer Cell*. 2010; 18:459–471. [PubMed: 21075311]
17. Christopher SA, Diegelman P, Porter CW, Kruger WD. Methylthioadenosine phosphorylase, a gene frequently codeleted with p16 (CDKN2A/ARF), acts as a tumor suppressor in a breast cancer cell line. *Cancer Res*. 2002; 62:6639–6644. [PubMed: 12438261]
18. Teng DH, et al. Human mitogen-activated protein kinase kinase 4 as a candidate tumor suppressor. *Cancer Res*. 1997; 57:4177–4182. [PubMed: 9331070]
19. Hollestelle A, et al. Distinct gene mutation profiles among luminal-type and basal-type breast cancer cell lines. *Breast Cancer Res. Treat*. 2010; 121:53–64. [PubMed: 19593635]
20. Shen R, Olshen AB, Ladanyi M. Integrative clustering of multiple genomic data types using a joint latent variable model with application to breast and lung cancer subtype analysis. *Bioinformatics*. 2009; 25:2906–2912. [PubMed: 19759197]
21. Tibshirani R, Hastie T, Narasimhan B, Chu G. Diagnosis of multiple cancer types by shrunken centroids of gene expression. *Proc. Natl Acad. Sci. USA*. 2002; 99:6567–6572. [PubMed: 12011421]
22. Kapp AV, Tibshirani R. Are clusters found in one dataset present in another dataset? *Biostatistics*. 2007; 8:9–31. [PubMed: 16613834]
23. Hughes-Davies L, et al. EMSY links the BRCA2 pathway to sporadic breast and ovarian cancer. *Cell*. 2003; 115:523–535. [PubMed: 14651845]
24. Brown LA, et al. Amplification of 11q13 in ovarian carcinoma. *Genes Chromosom. Cancer*. 2008; 47:481–489. [PubMed: 18314909]
25. Russnes HG, et al. Genomic architecture characterizes tumor progression paths and fate in breast cancer patients. *Sci. Transl. Med*. 2010; 2:38ra47.
26. Blows FM, et al. Subtyping of breast cancer by immunohistochemistry to investigate a relationship between subtype and short and long term survival: a collaborative analysis of data for 10,159 cases from 12 studies. *PLoS Med*. 2010; 7:e1000279. [PubMed: 20520800]
27. Mahmoud SMA, et al. Tumor-infiltrating CD8<sup>+</sup> lymphocytes predict clinical outcome in breast cancer. *J. Clin. Oncol*. 2011; 29:1949–1955. [PubMed: 21483002]
28. Daniel J, Coulter J, Woo J-H, Wilsbach K, Gabrielson E. High levels of the Mps1 checkpoint protein are protective of aneuploidy in breast cancer cells. *Proc. Natl Acad. Sci. USA*. 2011; 108:5384–5389. [PubMed: 21402910]
29. Chen Y, et al. Variations in DNA elucidate molecular networks that cause disease. *Nature*. 2008; 452:429–435. [PubMed: 18344982]

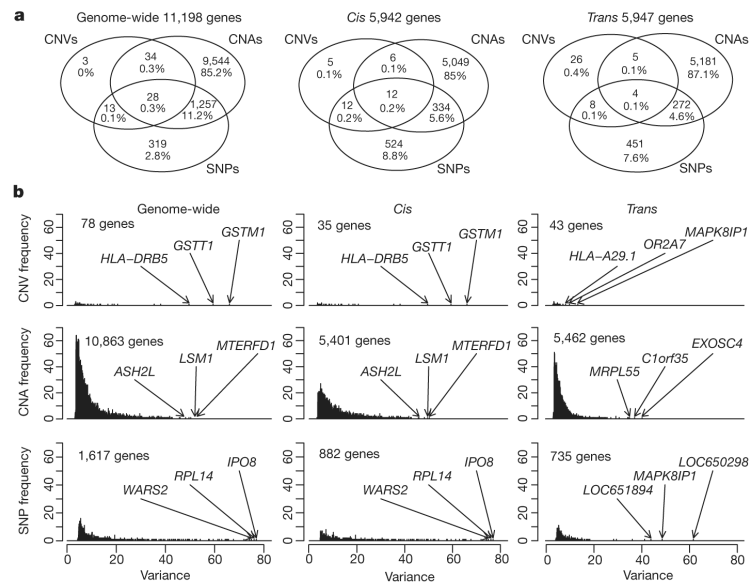


**Figure 1. Germline and somatic variants influence tumour expression architecture**

**a**, Venn diagrams depict the relative contribution of SNPs, CNVs and CNAs to genome-wide, *cis* and *trans* tumour expression variation for significant expression associations (Šidák adjusted  $P$ -value 0.0001).

**b**, Histograms illustrate the proportion of variance explained by the most significantly associated predictor for each predictor type, where several of the top associations are indicated.

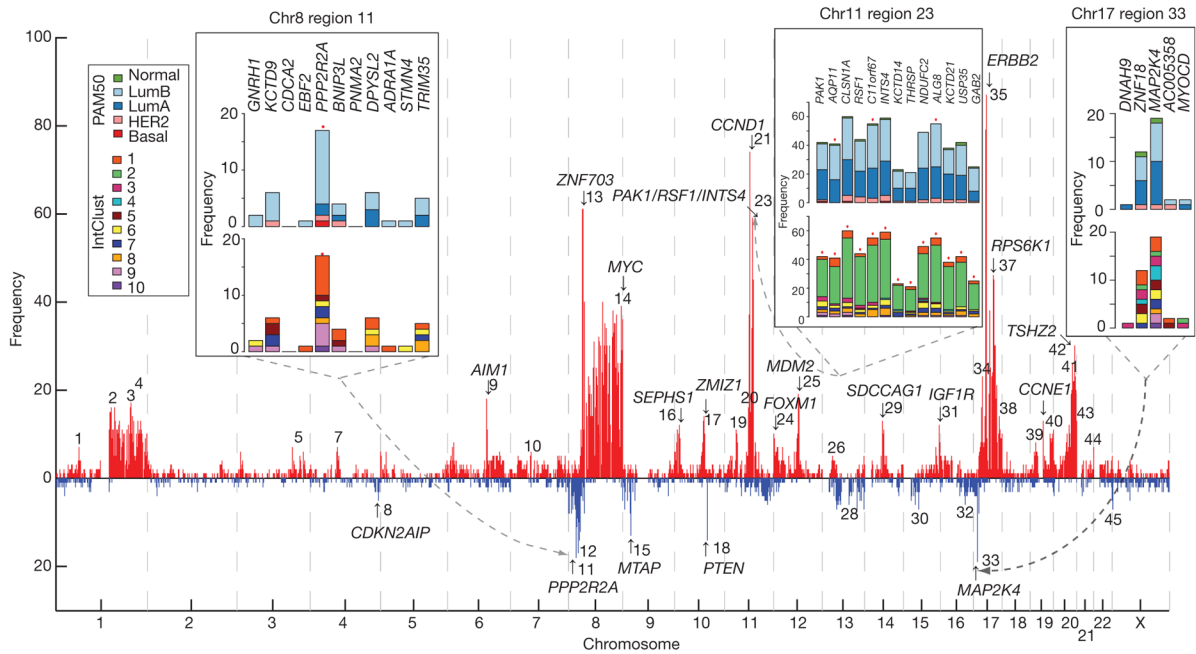


### Figure 2. Patterns of *cis* outlying expression refine putative breast cancer drivers

A genome-wide view of outlying expression coincident with extreme copy number events in the CNA landscape highlights putative driver genes, as indicated by the arrows and numbered regions. The frequency (absolute count) of cases exhibiting an outlying expression profile at regions across the genome is shown, as is the distribution across subgroups for several regions in the insets. High-level amplifications are indicated in red and homozygous deletions in blue. Red asterisks above the bar plots indicate significantly different observed distributions than expected based on the overall population frequency ( $\chi^2$  test,  $P < 0.0001$ ).

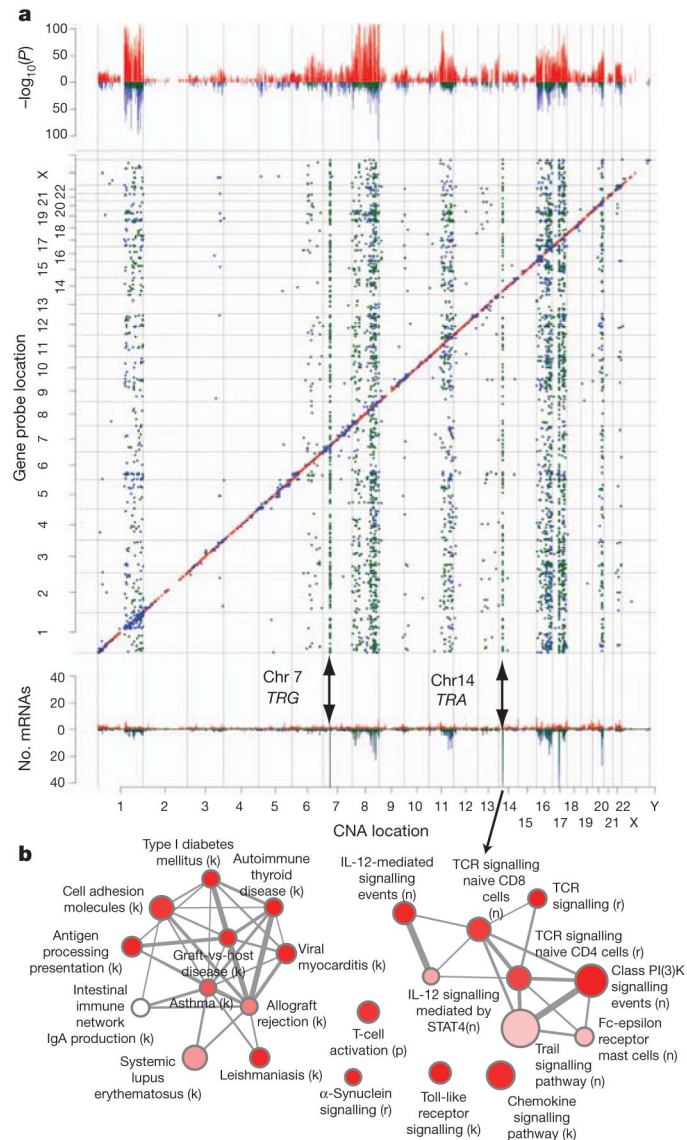


**Figure 3. Trans-acting aberration hotspots modulate concerted molecular pathways**

**a**, Manhattan plot illustrating *cis* and *trans* expression-associated copy number aberrations from the eQTL analysis (top panel). The matrix of significant predictor–expression associations (adjusted  $P$ -value  $< 0.0001$ ) exhibits strong off-diagonal patterns (middle panel), and the frequency of mRNAs associated with a particular copy number aberration further illuminates these *trans*-acting aberration hotspots (bottom panel). The directionality of the associations is indicated as follows: *cis*: positive, red; negative, pink; *trans*: positive, blue; negative, green. **b**, Enrichment map of immune response modules in the *trans*-associated TRA network, where letters in parentheses represent the source database as follows: b, NCI-PID BioCarta; c, cancer cell map; k, KEGG; n, NCI-PID curated pathways; p, PANTHER; r, Reactome.

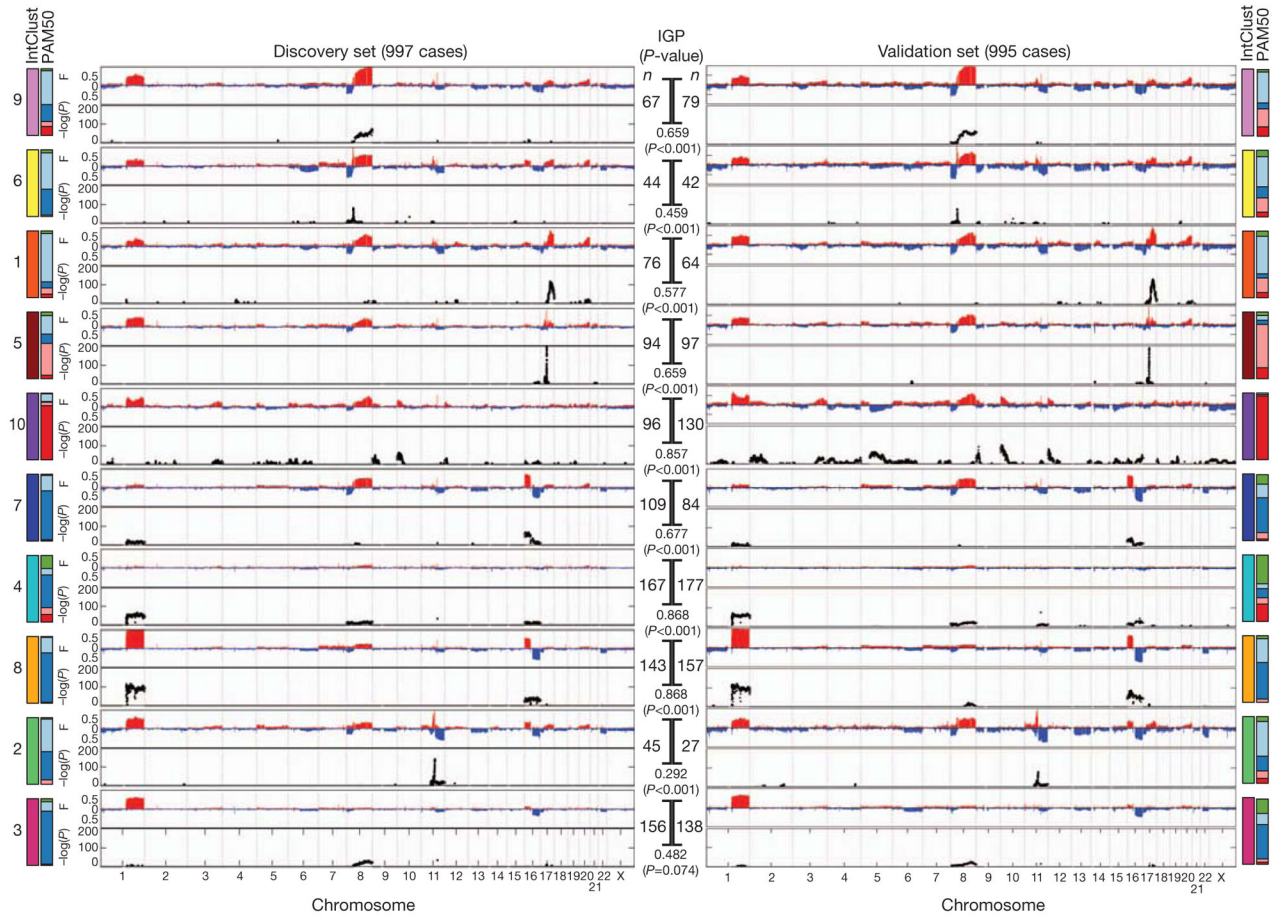


#### Figure 4. The integrative subgroups have distinct copy number profiles

Genome-wide frequencies (F, proportion of cases) of somatic CNAs ( $y$ -axis, upper plot) and the subtype-specific association ( $-\log_{10} P$ -value) of aberrations ( $y$ -axis, bottom plot) based on a  $\chi^2$  test of independence are shown for each of the 10 integrative clusters. Regions of copy number gain are indicated in red and regions of loss in blue in the frequency plot (upper plot). Subgroups were ordered by hierarchical clustering of their copy number profiles in the discovery cohort ( $n = 997$ ). For the validation cohort ( $n = 995$ ), samples were classified into each of the integrative clusters as described in the text. The number of cases in each subgroup ( $n$ ) is indicated as is the in-group proportion (IGP) and associated  $P$ -value, as well as the distribution of PAM50 subtypes within each cluster.

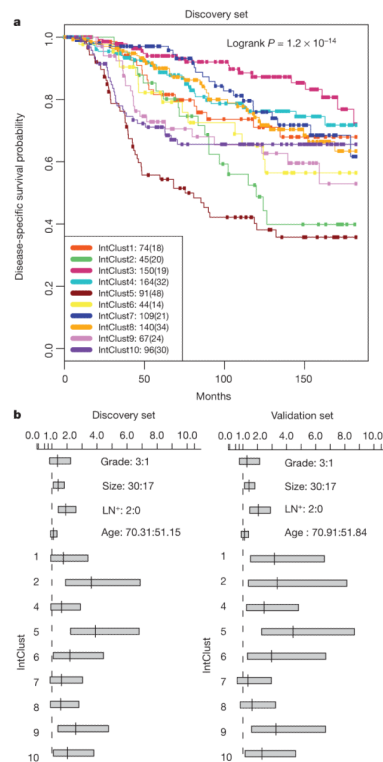


**Figure 5. The integrative subgroups have distinct clinical outcomes**

**a**, Kaplan–Meier plot of disease-specific survival (truncated at 15 years) for the integrative subgroups in the discovery cohort. For each cluster, the number of samples at risk is indicated as well as the total number of deaths (in parentheses). **b**, 95% confidence intervals for the Cox proportional hazard ratios are illustrated for the discovery and validation cohort for selected values of key covariates, where each subgroup was compared against IntClust 3.